International Journal of Heat and Mass Transfer 54 (2011) 1369–1386

Contents lists available at ScienceDirect

International Journal of Heat and Mass Transfer

journal homepage: www.elsevier.com/locate/ijhmt

Natural convection in a partially open square cavity with internal heat source: An analysis of the opening mass flow

Éliton Fontana [a], Adriano da Silva [b], Viviana Cocco Mariani [c,*]

[a] Universidade Federal de Santa Catarina, Departamento de Engenharia Química e de Alimentos, 88040-970 Florianópolis, SC, Brazil
[b] Universidade Federal de São João Del Rei, Campus Centro-Oeste Dona Lindu, 35501-296 Divinópolis, MG, Brazil
[c] Pontifícia Universidade Católica do Paraná, Programa de Pós-Graduação em Eng. Mecânica, 80215-901 Curitiba, PR, Brazil

ARTICLE INFO

Article history:
Received 10 October 2010
Received in revised form 10 November 2010
Accepted 10 November 2010
Available online 12 January 2011

Keywords:
Natural convection
Rayleigh numbers
Square cavity
Heat source
Heat transfer
Finite volume method

ABSTRACT

A steady buoyancy-driven flow of air in a partially open square 2D cavity with internal heat source, adiabatic bottom and top walls, and vertical walls maintained at different constant temperatures is investigated numerically in this work. A heat source with 1% of the cavity volume is present in the center of the bottom wall. The cold right wall contains a partial opening occupying 25%, 50% or 75% of the wall. The influence of the temperature gradient between the verticals walls was analyzed for $Ra_e = 10^3$–10^5, while the influence of the heat source was evaluated through the relation $R = Ra_i/Ra_e$, investigated at between 400 and 2000. Interesting results were obtained. For a low Rayleigh number, it is found that the isotherm plots are smooth and follow a parabolic shape indicating the dominance of the heat source. But as the Ra_e increases, the flow slowly becomes dominated by the temperature difference between the walls. It is also observed that multiple strong secondary circulations are formed for fluids with a small Ra_e whereas these features are absent at higher Ra_e. The comprehensive analysis is concluded with horizontal air velocity and temperature plots for the opening. The numerical results show a significant influence of the opening on the heat transfer in the cavity.

1. Introduction

In recent decades, research on natural convection in cavities has been the subject of many studies. Natural convection in open cavities and slots is encountered in many engineering applications, such as solar thermal receivers, heat convection from extended surfaces in heat exchangers, and solar energy collectors with insulated strips [1]. Cavities with a side opening and internal heat source can be seen in many electronic devices, where the openings facilitate the cooling of the internal components of the apparatus. Furthermore, the study of this case is relevant in many other applications, among which can be cited: construction and operation of nuclear reactors, solar energy collectors, energy storage systems, design and construction of indoor environments, and grain storage. Many studies have been reported in the literature, where the behavior of fluids within the cavities was evaluated, some of which are cited below.

The natural convection in cavities induced by the difference in temperature between vertical (or horizontal) walls is a case widely studied [2–15]. In those studies, the authors evaluated the influence of the temperature difference [2–5,7–12], aspect ratio, opening and inclinations of the cavity [6,13,15] on the fluid thermal behavior inside it. A numerical study on heat distribution and thermal mixing during steady laminar natural convective flow within fluid-saturated porous square cavities has been considered for three different cases: uniformly heated bottom wall, discrete heat sources on walls, and uniformly heated left and bottom walls in Kaluri et al. [10]. Deng and Chang [11] study numerically a two-dimensional steady and laminar natural convection in an air-filled rectangular enclosure where the horizontal walls are thermally insulated and the vertical side walls have two spatially varying sinusoidal temperature distributions of different amplitudes and phases. Michalek [12] conducted experiments to measure the water flow inside a cubical cavity with isothermal vertical walls and adiabatic horizontal walls for values of Ra_e greater than 10^9. The transition from stationary to non-stationary flow was below the theoretical value of the critical Rayleigh number. Bilgen and Oztop [13] performed a numerical study of heat transfer by natural convection in an inclined and partially open 2D cavity. A parametric study was conducted for values of Ra_e between 10^3 and 10^6, concluding that the value of Nusselt number was maximized for angles between 30° and 60° for low values of Ra_e, while at high values of Ra_e, the value of the Nusselt number was maximized for angles between 60° and 90°. Kuznik et al. [14] used the Lattice–Boltzmann method with a non-uniform mesh for the simulation of natural convection in a square cavity. The authors

* Corresponding author.
E-mail addresses: eliton_fontana@hotmail.com (É. Fontana), adrianodasilva.ufsj@gmail.com (A.da Silva), viviana.mariani@pucpr.br (V.C. Mariani).

0017-9310
doi:10.1016/j.ijheatmasstransfer.2010.11.053

Nomenclature

c_p	heat capacity at constant pressure (J/K)
g	gravity acceleration (m/s^2)
H	height of the cavity (m)
H^*	height of the opening (m)
k	thermal conductivity (W/m K)
Nu_C	Nusselt number on cold wall
Nu_H	Nusselt number on hot wall
p	pressure (Pa)
$\dot{q}$	volumetric heat source (W/m^3)
R	internal to external Rayleigh numbers ratio = Ra_i/Ra_e
Ra_e	external Rayleigh number = $g\beta(T_H - T_C)H^3/\nu\alpha$
Ra_i	internal Rayleigh number = $g\beta qH^5/\nu\alpha k$
T	temperature (K)
T_C	cold temperature (K)
T_H	hot temperature (K)
u	velocity in x direction (m/s)
u^*	dimensionless velocity = $u/u_{\max}$
$u_{\max}$	maximum velocity for each Rayleigh number and opening height (m/s)
$\bar{u}_{\max}$	relative maximum velocity
v	velocity in y direction (m/s)
W	length of the cavity (m)
x	horizontal distance (m)
y	vertical distance (m)

Greek symbols

α	thermal diffusivity (m^2/s)
β	thermal expansion coefficient (1/K)
θ	dimensionless temperature = $(T - T_C)/(T_H - T_C)$
μ	dynamic viscosity (kg/m s)
ν	kinematic viscosity (m^2/s)
ρ	density (kg/m^3)
Ψ	stream function (m^2/s)
Ψ_{dim}	dimensionless stream function

Subscripts

f	fluid
s	source

determined the Rayleigh numbers for the transition region between 10^3 and 10^9, and observed a good agreement with those reported in the literature. The same method was used by Mezrhab et al. [15], where the influence of the cavity inclination and the existence of an internal partition were evaluated. There was a maximum reduction in heat transfer for the range of Rayleigh numbers between 6×10^3 and 2×10^4. Some study combine effect of radiation and natural convection in cavities differentially heated [16–18].

When there is an internal heat source in cavities large changes in the internal flow characteristics occur. Studies on natural convection in cavities with internal heat source can be found in Kuznetsov and Sheremet [19], Nakhi and Chamkha [20], Oztop and Bilgen [21], Oztop and Abu-Nada [22], and Bazylak et al. [23], or with internal baffles in Fontana et al. [24]. In many cases, the cavity presents a partial opening, which facilitates mass flow and therefore the cooling process [25–29]. Mariani and Silva [28] conducted a numerical study of the thermal and fluid dynamics behavior of air in partially open 2D enclosures based on two aspects of the radius, $H/W = 1$ and 2. The enclosure had an opening on the right wall and a small heat source located on the bottom or left wall, occupying three different positions. Numerical simulations were performed for Ra_e in the range of 10^3 and 10^6 and it was found that changes in this parameter have significant effects on the average and local Nusselt numbers (Nu) of the enclosures. Another study was conducted by Mariani and Coelho [29] to investigate steady heat transfer and flow phenomena of natural convection of air in enclosures, with three aspect ratios ($H/W = 1$, 2, and 4), within which there is a local heat source on the bottom wall at three different positions. A similar study was carried out by Kandaswamy et al. [30], where the influence of the position and the size of the heat source were evaluated. This study was conducted for Grashof numbers between 10^3 and 10^5.

Hence, this study investigates natural convection in a partially open square cavity with an opening in the right wall of three different sizes $H/4$, $H/2$, and $3H/4$, where H is the cavity height. The cavity was submitted to temperature differences between the left and right vertical walls and had an internal heat conduction source. The influence of the internal heat source at intensities of $R = 400$, 1000 and 2000, and external Rayleigh numbers of $10^3 \leqslant Ra_e \leqslant 10^5$, on the thermal and fluid dynamics of the air inside the cavity and the mass inflow rate at the opening, was investigated. Local results are presented in the form of streamlines and isotherm plots, and the local Nusselt numbers on the hot and cold walls, providing valuable insight to the physical processes.

2. Mathematical formulation

Fig. 1 shows a schematic diagram of the problem under consideration and the coordinate system. The system to be considered is a two-dimensional square cavity of width W and height H, where the two vertical walls are kept at different temperatures, T_H (left

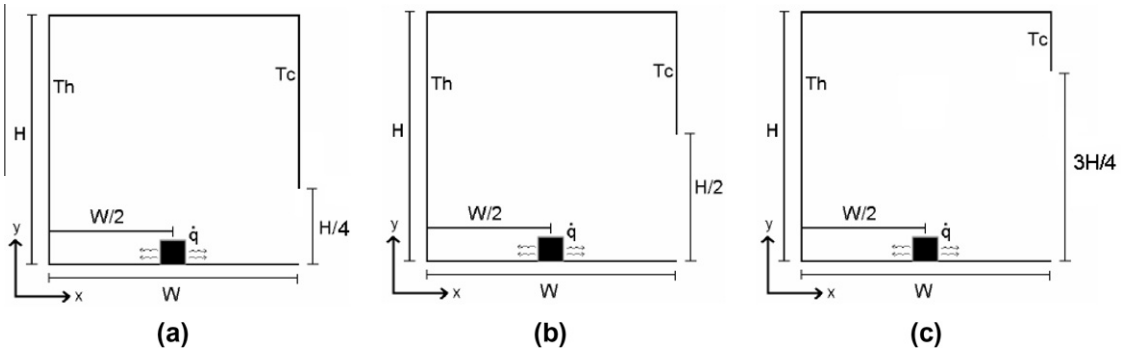

Fig. 1. Domain employed with opening placed on the right vertical wall of the cavity with sizes (a) $H/4$, (b) $H/2$, and (c) $3H/4$.

Table 1
Comparison of present prediction with previous results for natural convection in a closed square cavity without a heat source.

Grids	Authors	Ra_e	
		10^5	10^6
42×42	Hortmann et al. [31]	4.616	9.422
	Mariani and Silva [28]	4.605	9.487
	Present study	4.776	9.675
82×82	Hortmann et al. [31]	4.525	8.977
	Mariani and Silva [28]	4.535	8.975
	Present study	4.545	8.993

wall) and T_C (right wall), $T_H > T_C$. Zero heat flow is assumed at the top and bottom walls. The walls are rigid and no-slip conditions are imposed at the boundaries. The internal heat source is placed on the bottom horizontal wall, midway between the vertical walls, occupying 1% of the total volume of the cavity. The opening is placed on the right vertical wall of the cavity being evaluated for three conditions $H^* = H/4$, $H/2$, and $3H/4$.

The flow field is considered to be steady and the fluid is incompressible. Thermophysical properties of the fluid are assumed constant, with the exception of the density variation in the buoyancy

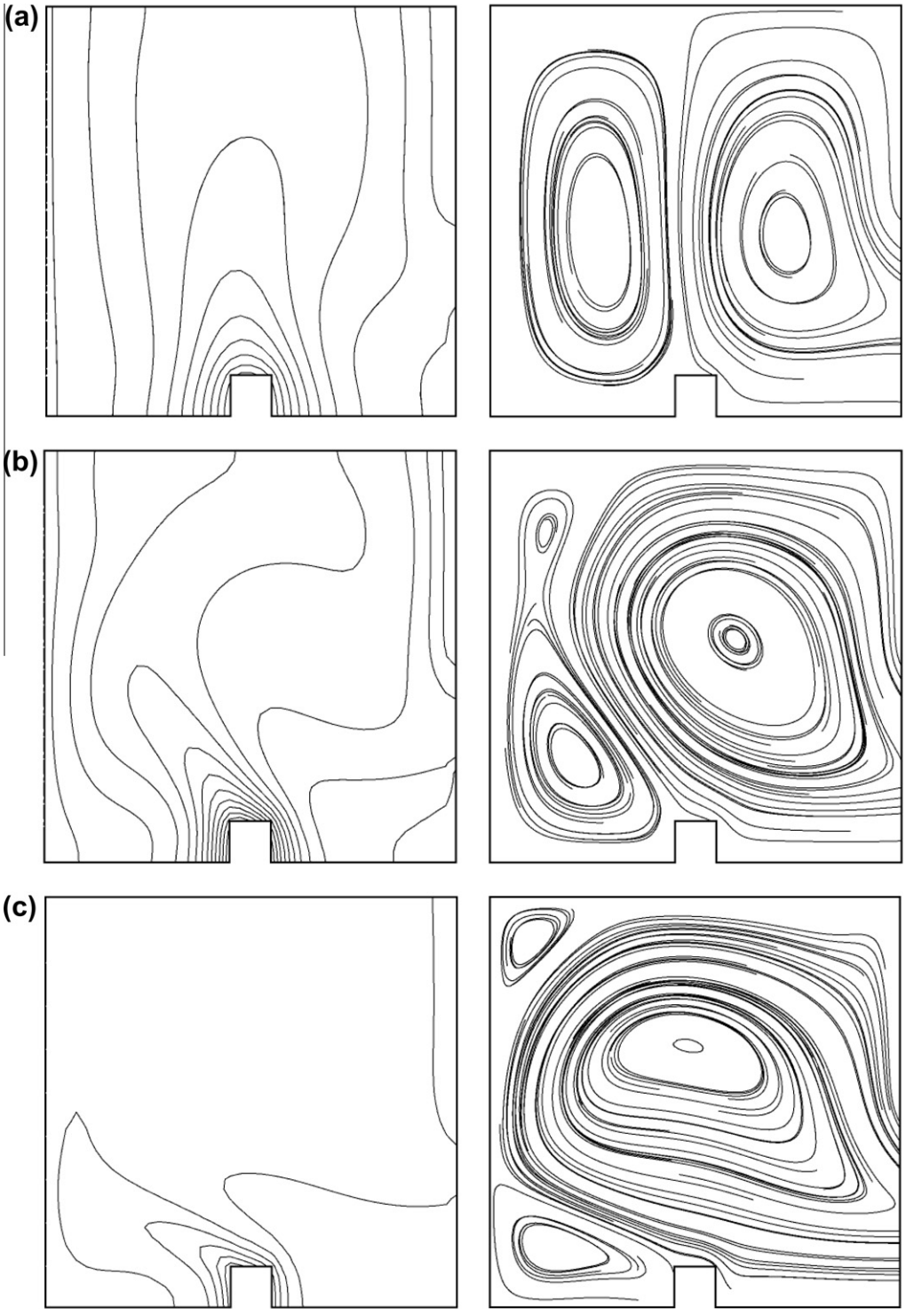

Fig. 2. Isotherms (left) and streamlines (right) for $R = 2500$ and (a) $Ra_e = 10^3$, (b) $Ra_e = 10^4$, and (c) $Ra_e = 10^5$.

Table 2
Dimensionless maximum temperature and computing time required for the grid selected in this study.

Grid	32 × 32	42 × 42	62 × 62	82 × 82	122 × 122	Unstructured
$Ra_e = 10^3$	3.532	3.538	3.538	3.538	2.538	3.538
$Ra_e = 10^4$	2.800	2.830	2.860	2.870	2.870	2.870
$Ra_e = 10^5$	2.183	2.216	2.293	2.340	2.342	2.345
Dimensionless time	1	1.43	4.37	6.56	13.55	28.05

term, i.e., the Boussinesq approximation is valid. The equations for the conservation of mass, momentum and energy are:

$$\frac{\partial u}{\partial x}+\frac{\partial v}{\partial y}=0, \tag{1}$$

$$\frac{\partial(uu)}{\partial x}+\frac{\partial(uv)}{\partial y}=-\frac{1}{\rho}\frac{\partial p}{\partial x}+\nu\left(\frac{\partial^2 u}{\partial x^2}+\frac{\partial^2 u}{\partial y^2}\right), \tag{2}$$

$$\frac{\partial(uv)}{\partial x}+\frac{\partial(vv)}{\partial y}=-\frac{1}{\rho}\frac{\partial p}{\partial y}+\nu\left(\frac{\partial^2 v}{\partial x^2}+\frac{\partial^2 v}{\partial y^2}\right)+g\beta(T-T_C), \tag{3}$$

$$\frac{\partial(uT)}{\partial x}+\frac{\partial(vT)}{\partial y}=\alpha\left(\frac{\partial^2 T}{\partial x^2}+\frac{\partial^2 T}{\partial y^2}\right)+\frac{\dot{q}}{\rho c_p}, \tag{4}$$

where the variables u, v and T are the velocity components in the x, y direction and temperature, respectively. The quantities ρ, $\alpha = k/\rho c_p$, $\nu = \mu/\rho$, and β are the density, thermal diffusivity, kinematic viscosity and thermal expansion coefficient of the fluid, respectively. The temperature was evaluated in dimensionless form as:

$$\theta=\frac{T-T_C}{T_H-T_C} \tag{5}$$

where T_C is cold temperature and T_H is hot temperature. The boundary conditions used are:

$$u=v=0, \quad \text{and} \quad \theta=0 \quad \text{in } x=W; \quad H^*\leqslant y\leqslant H, \tag{6}$$

$$u=v=0, \quad \text{and} \quad \theta=1 \quad \text{in } x=0; \quad 0\leqslant y\leqslant H, \tag{7}$$

$$u=v=0, \quad \text{and} \quad \partial\theta/\partial y=0 \quad \text{in } 0\leqslant x\leqslant W=0; \quad y=0, \tag{8}$$

$$u=v=0, \quad \text{and} \quad \partial\theta/\partial y=0 \quad \text{in } 0\leqslant x\leqslant W=0; \quad y=H, \tag{9}$$

$$k_s\partial\theta_s/\partial n=k_f\partial\theta_f/\partial n \text{ at the source–fluid interface}, \tag{10}$$

where the subscript s denotes the source, the subscript f denotes the fluid, and H^* denotes the opening height.

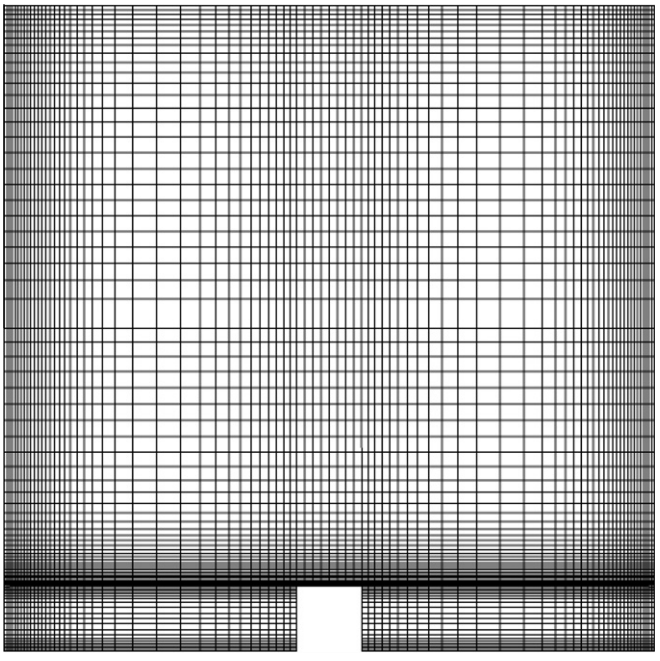

Fig. 3. Mesh with 82 × 82 control volumes.

The external Rayleigh number is represented by the difference in temperature between the vertical walls, $10^3 \leqslant Ra_e \leqslant 10^5$, defined as:

$$Ra_e=\frac{g\beta(T_H-T_C)H^3}{\nu\alpha}, \tag{11}$$

and the intensity of heat produced by the source heat is represented by the internal Rayleigh number, Ra_i, which is based on the volumetric heat-generation rate:

$$Ra_i=\frac{g\beta qH^5}{\nu\alpha k}. \tag{12}$$

The influence of the intensity of the two Rayleigh numbers is evaluated by means of the relation:

$$R=\frac{Ra_i}{Ra_e}, \tag{13}$$

where the values for R are 400, 1000 and 2000.

Other physical quantities of interest in the present study are the local Nusselt numbers along the hot and cold walls and the average Nusselt number. The local Nusselt numbers are defined, respectively, as:

$$Nu_H=\left.\frac{\partial\theta}{\partial X}\right)_{X=0}, \tag{14}$$

$$Nu_C=\left.\frac{\partial\theta}{\partial X}\right)_{X=W}, \tag{15}$$

The stream function is defined as:

$$u=\frac{\partial\Psi}{\partial Y}, \tag{16}$$

$$v=-\frac{\partial\Psi}{\partial X}. \tag{17}$$

However, the numerical results are presented in terms of the dimensionless stream function given by:

$$\Psi_{dim}=\frac{\Psi}{\alpha}. \tag{18}$$

The air velocity at the open right wall is evaluated by the dimensionless velocity defined as:

$$u^*=\frac{u}{u_{\max}}, \tag{19}$$

Table 3
Maximum dimensionless temperature for different configurations.

Parameters	Opening size			
R	Ra_e	$H/4$	$H/2$	$3H/4$
400	10^3	3.473	3.538	3.565
	10^4	2.765	2.879	2.919
	10^5	2.326	2.331	2.370
1000	10^3	7.005	7.077	7.211
	10^4	5.353	5.485	5.715
	10^5	3.710	3.812	3.924
2000	10^3	11.047	11.500	12.199
	10^4	8.033	8.138	9.499
	10^5	5.368	5.643	5.808

where u_{max} is the maximum velocity for each Rayleigh number and opening height used. The velocity is calculated as a function of the dimensionless height given by:

$$Y^* = \frac{Y}{H}, \tag{20}$$

where H is the cavity height.

The relative maximum velocity, $\bar{u}_{max}$, gives the relation between the maximum velocity and the maximum velocity for $Ra_e = 10^3$ with opening $H^* = H/4$

$$\bar{u}_{max} = \frac{u_{max}}{u^*_{max}}. \tag{21}$$

3. Numerical method

Based on the above assumptions, the conservation equations (Eqs. (1)–(4)) together with the boundary conditions (Eqs. (6)–(10)) were solved by the finite volume CFD commercial package ANSYS CFX version 11.0. A base, non equal-spaced, grid of 82×82 (first cell dimension = 3×10^{-3} L) was used, the expansion factor variable using exponential and non-linear functions for the points selected as a trade-off between numerical accuracy and computation time. The High Resolution Differencing Scheme was employed for $Pr = 0.71$. A 0.5 under relaxation factor was used only for the mass, momentum and energy equations (Eqs. (1)–(4)). The resulting discrete system of linear equations is solved using an algebraic multigrid methodology called the additive correction accelerated incomplete lower upper (ILU) factorization technique. This is an iterative solver whereby the exact solution of the equations is approached during the course of several iterations. Finally, the solution was considered converged when the sum of absolute normalized residuals for all cells in the flow domain became less than 10^{-7}.

The numerical procedure was validated by comparison with the results provided by Hortmann et al. [31] and Mariani and

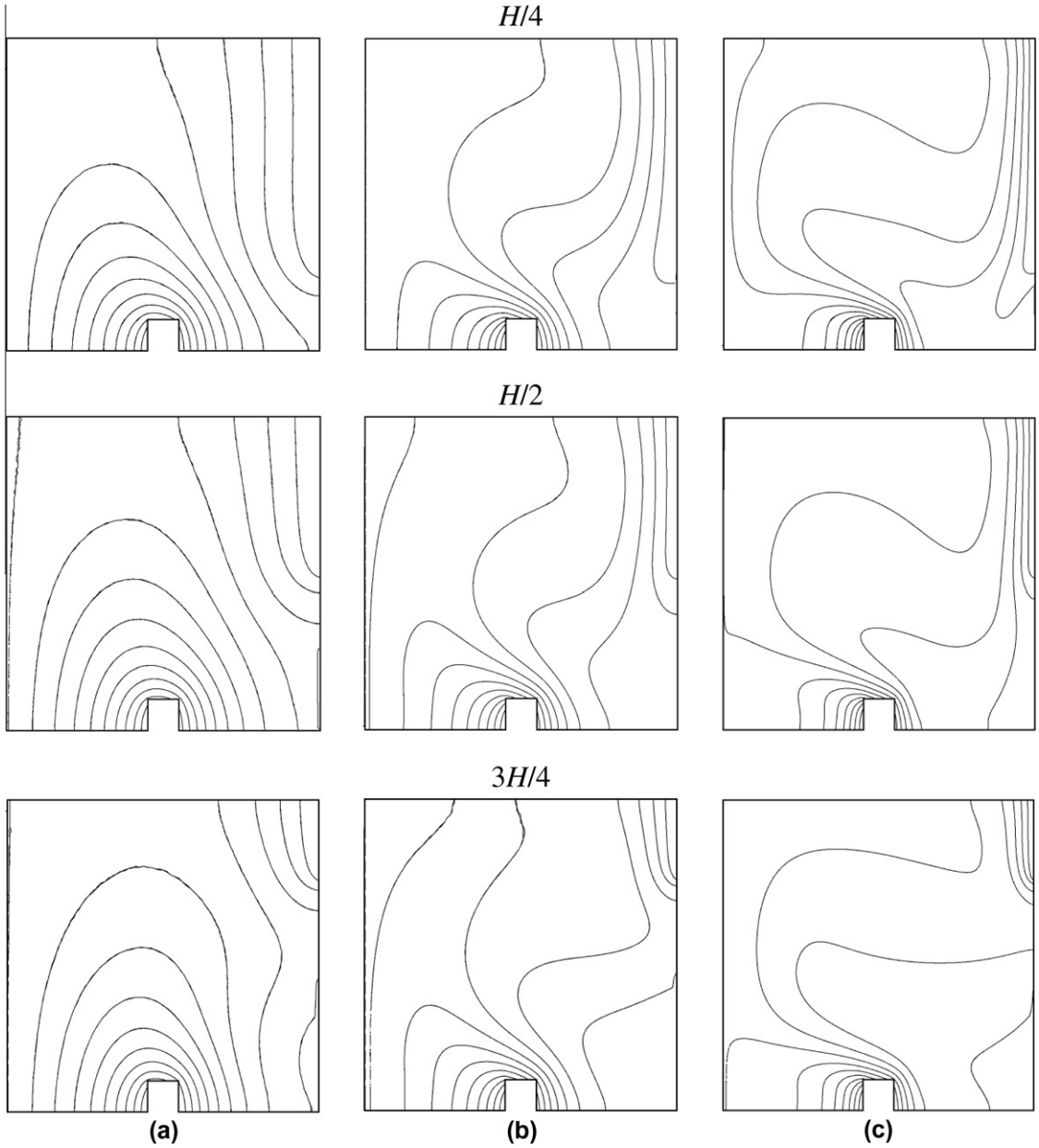

Fig. 4. Isotherms for $R = 400$ for (a) $Ra_e = 10^3$, (b) $Ra_e = 10^4$, and (c) $Ra_e = 10^5$.

Silva [28]. These results were obtained under natural convection in a closed square cavity without a heat conduction source. The results for the average Nusselt number for two meshes, 42×42 and 82×82, and for two Rayleigh numbers, 10^3 and 10^6, are summarized in Table 1. A very good agreement between the present predictions and those provided by Hortmann et al. [31] and Mariani and Silva [28] can be observed. The numerical results shown in Table 1 were compared with the results of Hortmann et al. [31] and Mariani and Silva [28] presenting mean standard deviations of 2.87% for a 42×42 grid and 0.26% for an 82×82 grid.

Further comparison of the numerical results was carried out by presenting the local results in the form of the streamline and isotherm plots of Xia and Zhou [32] for $R = 2500$ and an opening of $H/2$, as shown in Fig. 2. Note that the numerical results obtained in this study are in good agreement with those of Xia and Zhou [32], although small differences can be noted because in this study an average temperature in the cavity opening was used while in the previous study the cold temperature in the cavity opening was employed.

In order to determine the number of volumes required to obtain a grid-independent solution, some numerical simulations were carried out. In fact, five structured computational grid levels were used, plus one unstructured grid for the physical domain. The refinement was mainly promoted at the walls of the cavity and next to the heat source, where the gradients are higher. The numerical validation was carried out using the results for the dimensionless maximum temperature for $R = 400$ and $10^3 \leqslant Ra_e \leqslant 10^5$ as detailed in Table 2.

The precision of the grids was analyzed by comparing their predicted results. Besides the accuracy, the computing cost is another important aspect related to the grid performance. Table 2 also lists the dimensionless computing time, i.e., the relation between the CPU times required for each grid. From these results, a structured mesh with 82×82 elements was selected, because the use of a

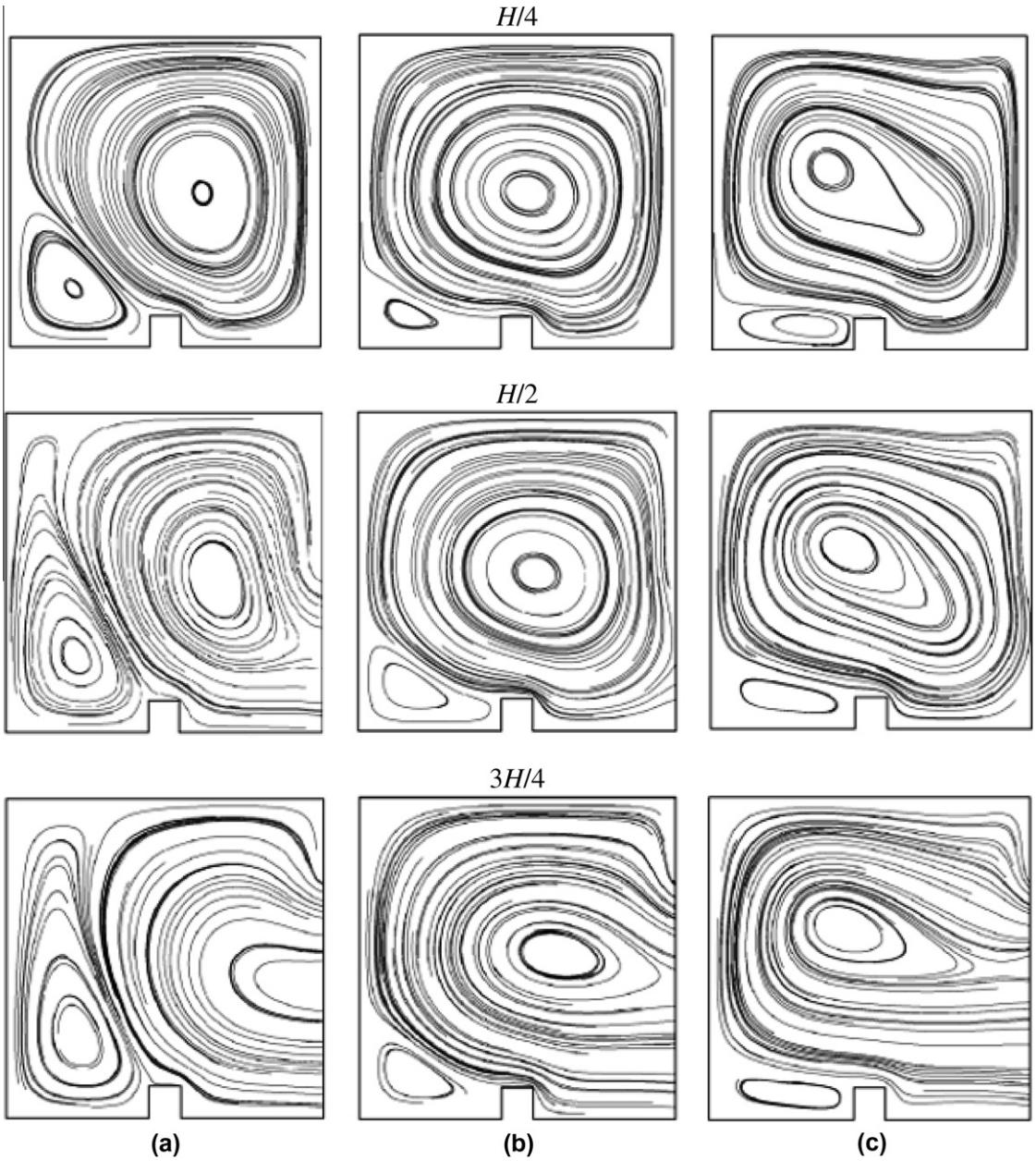

Fig. 5. Streamlines $R = 400$ for (a) $Ra_e = 10^3$, (b) $Ra_e = 10^4$, and (c) $Ra_e = 10^5$.

more refined mesh does not affect the results and requires a long resolution time. The mesh used can be seen in Fig. 3.

4. Results and discussion

In the following sections, the heat transfer along the hot and cold walls, the air flow and the temperature fields are examined for external Rayleigh numbers of $Ra_e = 10^3$, 10^4, and 10^5, values for the relation between the external and internal Rayleigh numbers of $R = 400$, 1000, and 2000, and an opening in the right vertical wall of the square cavity with sizes of $H^* = H/4$, $H/2$, and $3H/4$.

The particularity of this problem is the appearance of different solutions when varying the parameters R, Ra_e and H^*. The air flow structure is mainly composed of closed cells which are due to the upward recirculating movement of the air inflow or to natural convection phenomena.

4.1. Maximum temperature results

We note that in some cases the materials inside the cavity are sensitive to high temperatures, for example, electronic components where chips may suffer damage if the temperature is high at some point. Table 3 gives the results obtained for the maximum dimensionless temperature simulation of all configurations studied herein. According to Table 3, for all R values investigated the maximum dimensionless temperature decreases with increasing Ra_e because it makes the air move with greater velocity in the cavity, facilitating heat exchange. For small values of Ra_e, the air next to the heat source is more stagnant, thus increasing the temperature.

As the value of R increases there is a considerable increase in the maximum temperature for all values of Ra_e. This is due to the fact that the maximum temperature is reached in the region next to the heat source, thus increasing the influence of the heat source on the

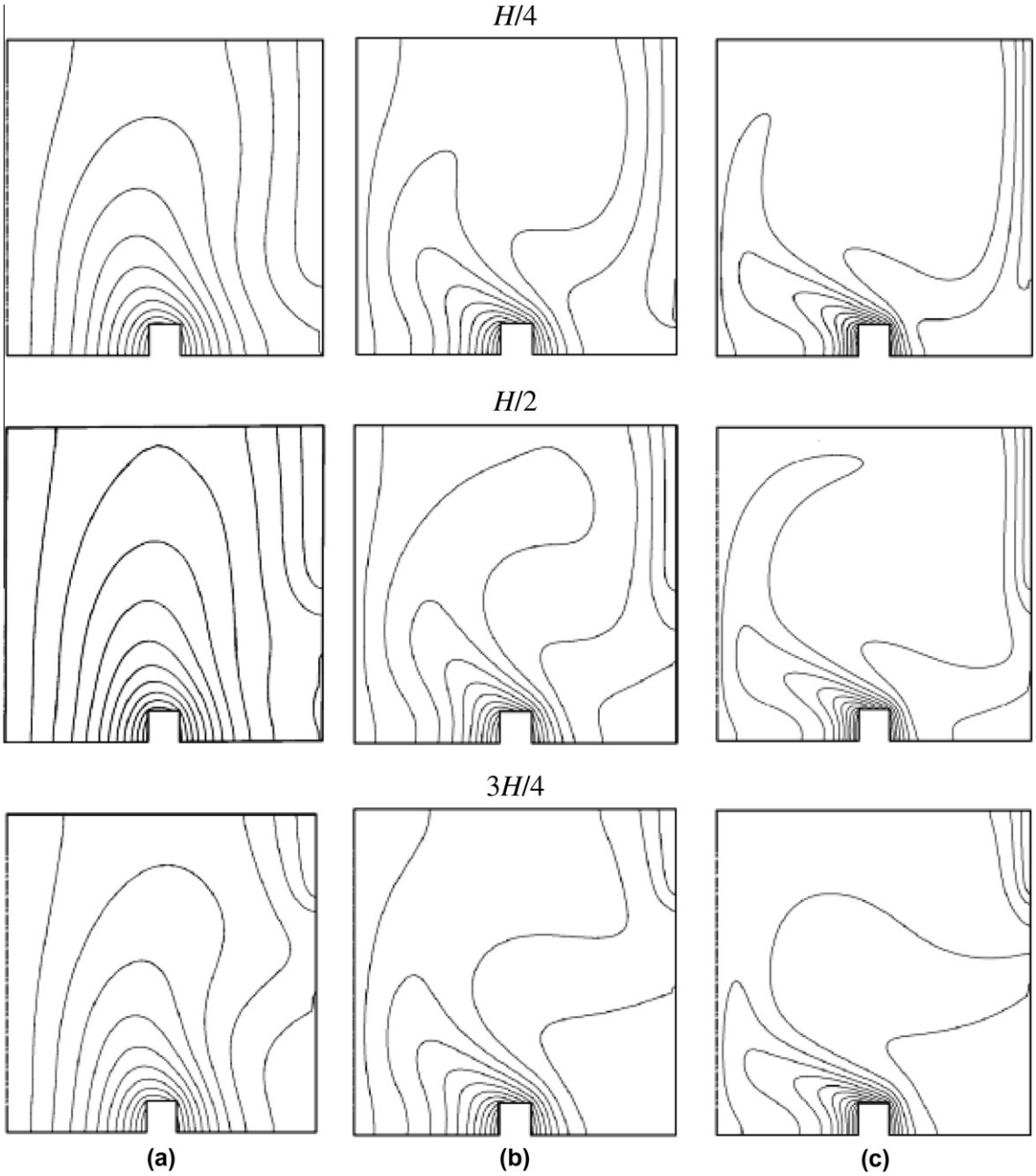

Fig. 6. Isotherms for $R = 1000$ for (a) $Ra_e = 10^3$, (b) $Ra_e = 10^4$, and (c) $Ra_e = 10^5$.

wall temperatures (measured by R values), with a relative increase in temperature in this region. Generally, on increasing the opening size there is an increase in the value of the maximum temperature due to a reduction in the area of heat exchange between the air and the cold wall. Therefore, it is noted that the main factor responsible for the air cooling is the cold wall.

4.2. Flow structure and isotherms

The flow structure and the thermal field are, respectively, represented by the isotherms and streamlines in Figs. 4 and 5, for all Rayleigh numbers and opening sizes, for $R = 400$. For a low Rayleigh number, $Ra_e = 10^3$, Fig. 4a, the isotherm is smooth and the distribution of temperature follows a parabolic shape, behavior typical of a cavity with an internal heat source and with no temperature difference between the walls. On the other hand, for a higher Rayleigh number, $Ra_e = 10^5$, Fig. 4c, the isotherm lines are more horizontal, this behavior being characteristic of a cavity with vertical walls kept at different temperatures and with no heat source. It can be observed that, when the opening size is $H/2$ or $3H/4$ there is a similar behavior of the isotherm plots for the higher values of Ra_e studied ($Ra_e = 10^4$ and 10^5). This occurs due to the decrease in the size of the cold wall and, hence, the flow and heat transfer will be controlled by the internal heat source, and the difference in the temperatures of the vertical walls has a smaller influence. The temperature distribution inside the cavity for an opening size of 50% is similar to that obtained using an opening size of 25%, particularly for a Rayleigh number of 10^3.

An analysis of Fig. 5 indicates that when $Ra_e = 10^5$ or 10^4, Fig. 5c and b, there is one strong primary rotating cell at the center of the cavity, and a smaller weaker cell near the bottom left of the cavity next to the heat source, for all opening sizes investigated. Note that the circulation close to the heated wall is less intense than the main circulation, because the heat source begins to lose its importance to the difference in temperature between the vertical walls.

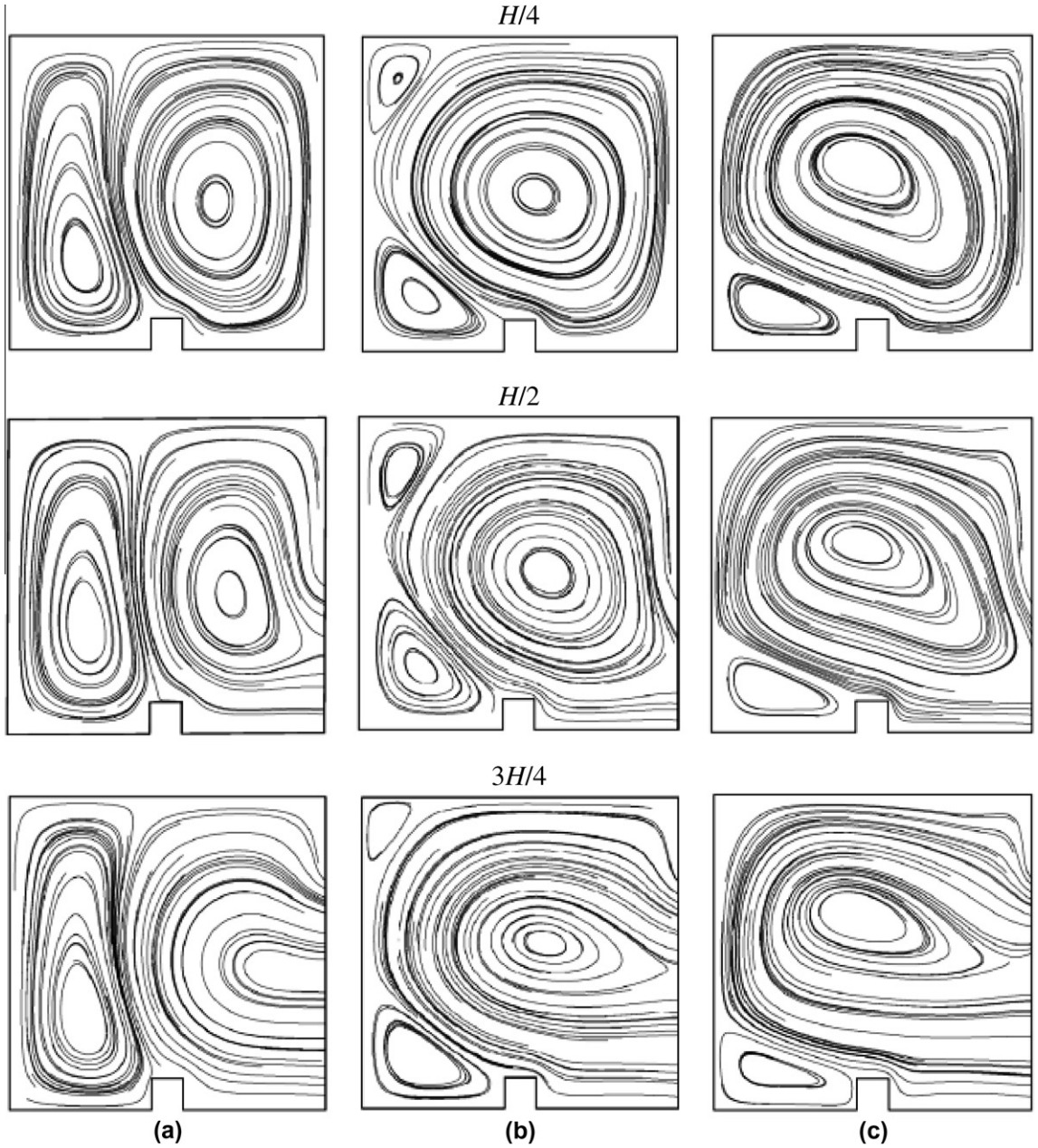

Fig. 7. Streamlines for $R = 1000$ for (a) $Ra_e = 10^3$, (b) $Ra_e = 10^4$, and (c) $Ra_e = 10^5$.

For the highest opening size, a further decrease in Ra_e to 10^3 completely divides the cavity and results in a pair of strong cells, one clockwise rotating cell in the right half of the cavity and another counterclockwise in the left half, where the intensity of both eddies is important. Hence, the flow and heat transfer are controlled by the internal heat source, and the difference in the temperatures of the vertical walls has negligible influence. Also for $Ra_e = 10^3$, the secondary circulation cell is bigger than for the larger Rayleigh numbers.

Under these circumstances we found no significant change in the flow and heat transfer characteristics for $R = 400$ when maintaining the Rayleigh number, Ra_e, fixed at 10^4 or 10^5 for the smaller opening size studied. However, there are significant differences when $Ra_e = 10^3$ as a function of the opening size, i.e., significant changes in the fluid dynamics behavior are observed when the opening size is decreased from 50% or 75% to 25% (see Fig. 5a).

The isotherms and streamlines for $R = 1000$ are shown in Figs. 6 and 7, respectively, for Rayleigh numbers $Ra_e = 10^3$–10^5, and opening sizes $H^* = H/4$, $H/2$, and $3H/4$. On comparing Figs. 6 and 7 with Figs. 5 and 6, increases in the influence of the heat source can be noted. An analysis of these figures indicates that for any opening size various differences occur in the flow pattern, according to the change in Ra_e or R.

On analyzing Fig. 6, first fixing Ra_e at 10^3, one finds that, for all opening sizes, Fig. 6a, no significant changes are noted in the isotherm characteristics, and the distribution of temperature follows a parabolic shape. However, for the higher Rayleigh numbers, $Ra_e = 10^4$ and 10^5, Fig. 6b and c, the isotherms are more horizontal. When $Ra_e = 10^4$, Fig. 6b, the isotherms in the region next to the hot wall are affected main by the heat source, while in the region next to the opening the isotherms are influenced by the difference between the temperatures of the vertical walls, where more horizontal isotherms can be seen. Note that the increase in the heat source affects the isotherm behavior for $Ra_e = 10^5$, see Fig. 6c.

Now, from Fig. 7 it can be seen that when $Ra_e = 10^3$ the heat source of $R = 1000$, Fig. 7a, has more influence than in the case of

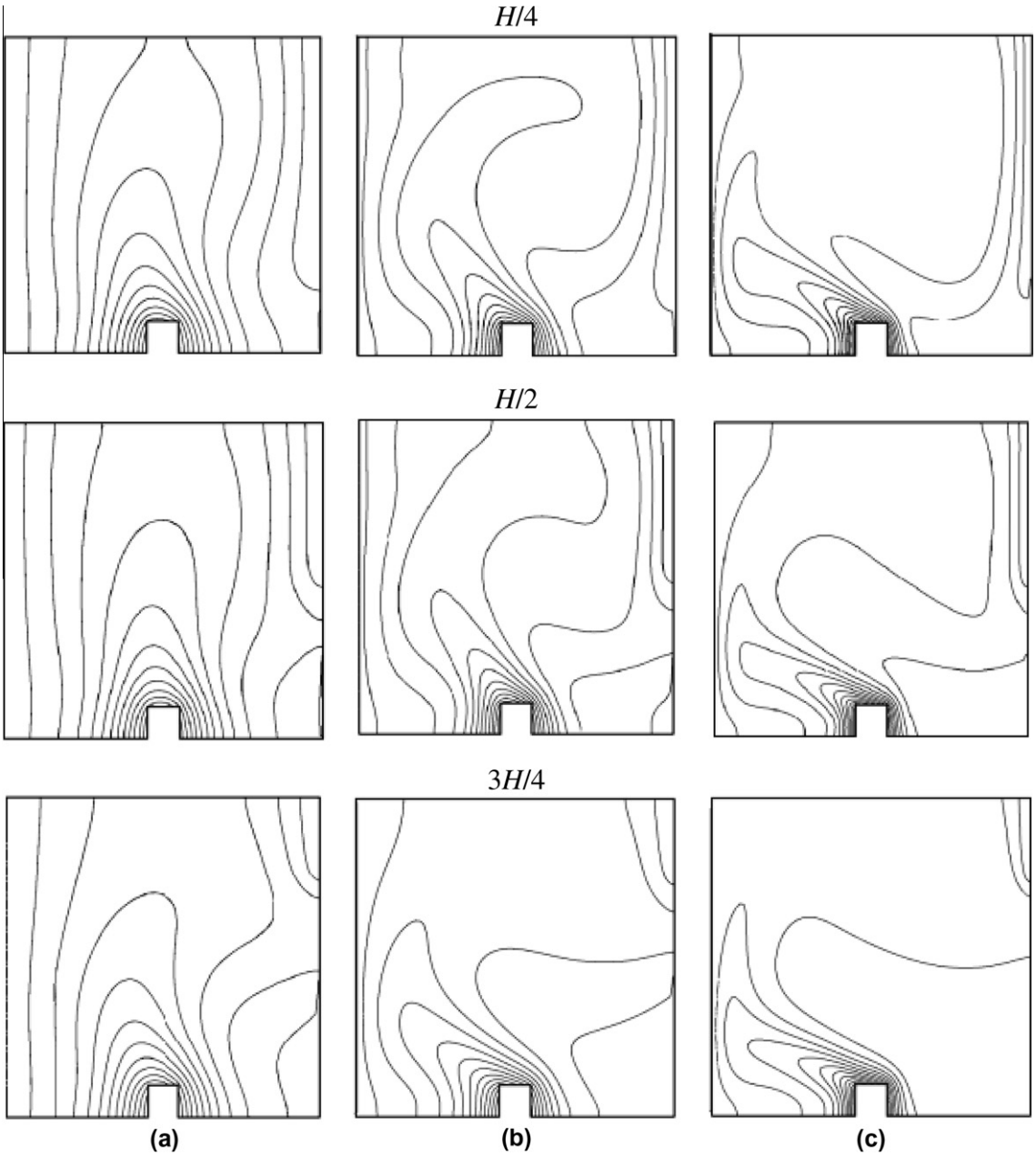

Fig. 8. Isotherms for $R = 2000$ for (a) $Ra_e = 10^3$, (b) $Ra_e = 10^4$, and (c) $Ra_e = 10^5$.

$R = 400$, Fig. 5a, for each opening size studied. In Fig. 7a also note that the secondary circulation is larger than that obtained with $R = 400$ although it is lower than the main circulation, indicating that for this case both the heat source and temperature difference between the vertical walls have considerable influence on the fluid dynamics of the air. The greatest influence was reflected in the intensity of the eddy formed between the heat source and the left vertical wall, particularly for an opening size of $H/4$. It should be noted that when $H^* = H/2$ or $3H/4$ the main rotating cell is not completely inside the cavity.

When $Ra_e = 10^4$, Fig. 7b, and for all opening sizes, two weaker rotating cells appear at the top and bottom left of the cavity. These cells are formed due to the influence of the heat source, but in general the fluid flow is controlled by the temperature difference between the vertical walls. Fig. 7c showed that when $Ra_e = 10^5$ no significant changes in the flow characteristics are noted. In this case the air flow is controlled by temperature difference between the vertical walls and the secondary circulation at the bottom left of the cavity increases.

Figs. 8 and 9 show the isotherms and streamlines, respectively, at $R = 2000$, for $Ra_e = 10^3$–10^5 and three opening sizes, $H/4$, $H/2$, and $3H/4$. On analyzing $Ra_e = 10^3$, Fig. 8a, it is clear that the isotherms in the cavity have parabolic characteristics for all opening sizes studied. This can be attributed to the fact that the temperature distribution is controlled by the heat source. From Fig. 8b, $Ra_e = 10^4$, it can be noted that a small opening has a greater influence on the isotherms. The isotherms for $Ra_e = 10^5$ indicate that the heat is conducted horizontally, mainly through the temperature difference between the vertical walls. Hence, the isotherms are not affected by the heat source. A comparison with isotherms obtained for $R = 400$ and 1000 reveals that the values for R studied here have relatively little influence on the flow and heat transfer for $Ra_e = 10^5$.

The value of $Ra_e = 10^3$, Fig. 9a, completely divides the cavity and results in a pair of strong rotating cells, one clockwise in the right half of the cavity and another counterclockwise in the left half of the cavity. These indicate that the flow pattern can be controlled mainly by the heat source. When $Ra_e = 10^4$, Fig. 9b, it can be seen

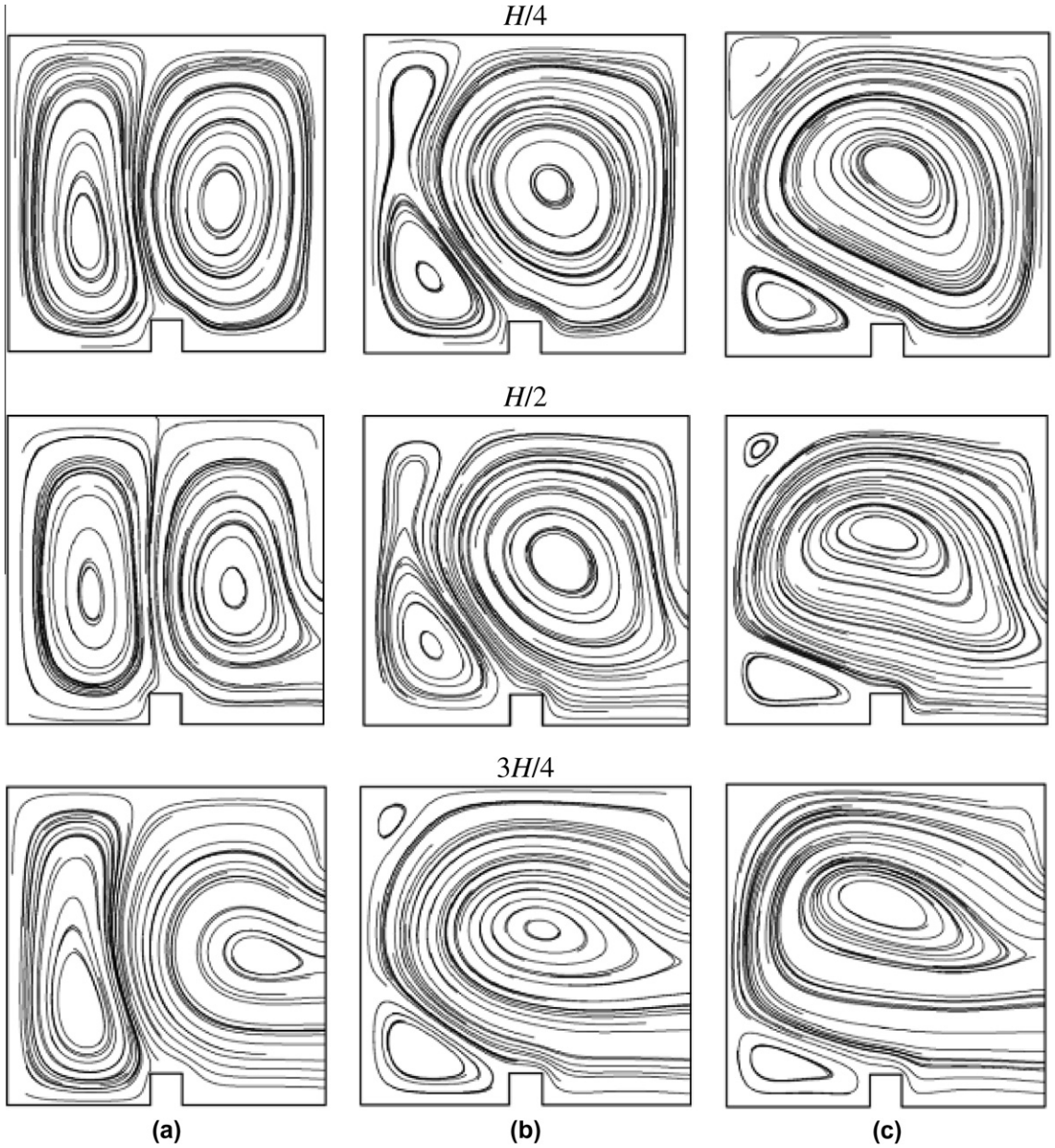

Fig. 9. Streamlines for $R = 2000$ for (a) $Ra_e = 10^3$, (b) $Ra_e = 10^4$, and (c) $Ra_e = 10^5$.

that besides the main rotating cell, another strong secondary rotating cell appears, for opening sizes of $H/4$ and $H/2$, indicating that in this case the flow pattern is influenced by the heat source and the temperature difference. When the opening size is $3H/4$ two weaker secondary rotating cells are observed next to the hot wall, at the bottom and top of the cavity, indicating the smaller influence of the heat source. In Fig. 9c, when $Ra_e = 10^5$, note that for all opening sizes investigated the flow pattern reflects the temperature difference between the vertical walls.

4.3. Heat transfer results

The quantitative heat transfer results are presented in terms of the local Nusselt number along the hot and cold walls of the square

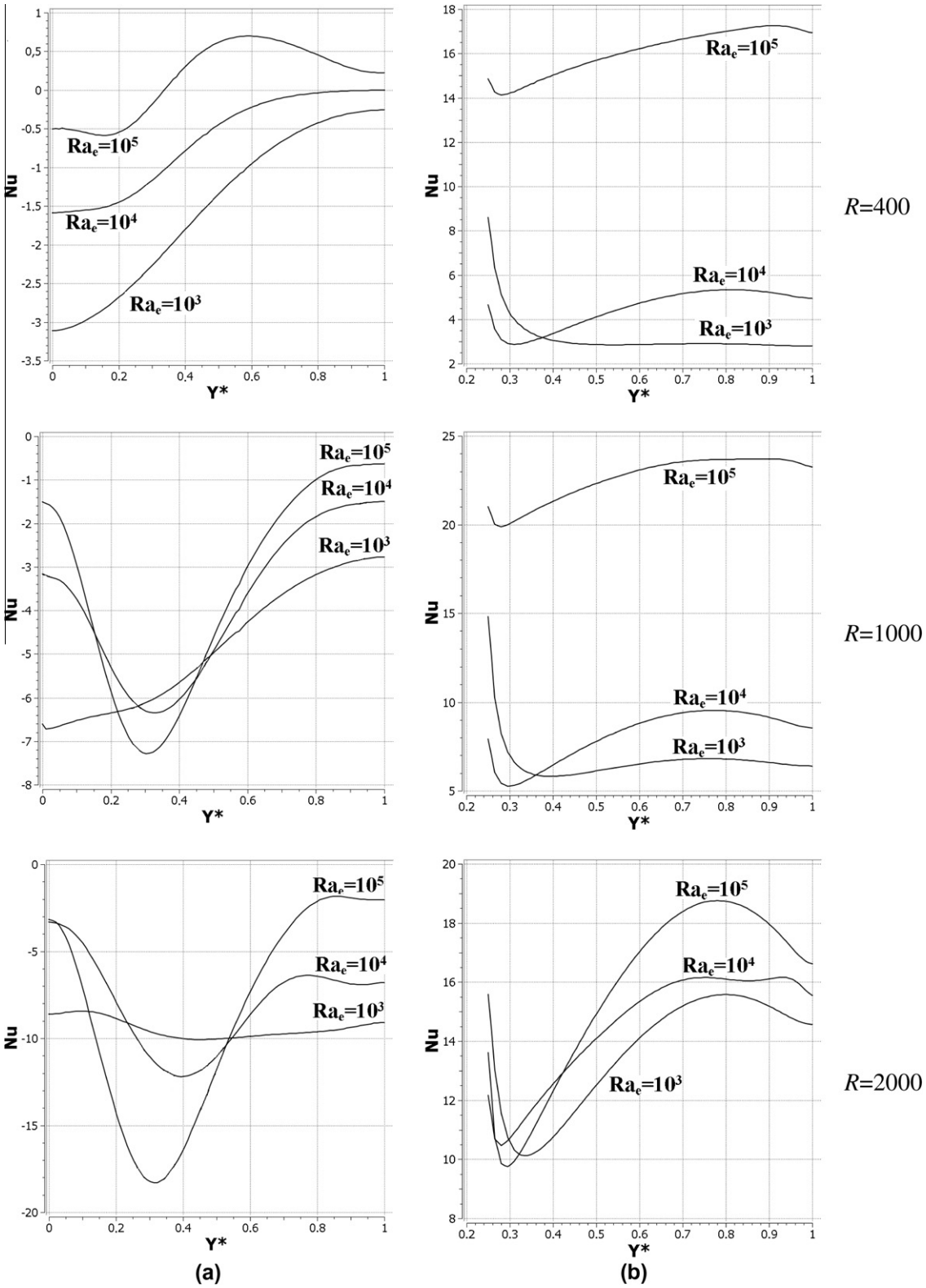

Fig. 10. Local Nusselt number along the (a) hot wall and (b) cold wall for an opening size of $H/4$.

cavity in Figs. 10–12. As can be seen, the curves for the two cases display different behaviors, the local Nusselt number along the cold wall reaching a maximum in the top part of the cavity, while along the hot wall it reaches a maximum in the bottom part of the cavity. It is also shown that increasing the opening size produces an increase (in modulus) in the two Nusselt numbers for $R = 400$, when the flow is controlled mainly by the temperature difference between the walls.

Indeed, the aspiration of air into the cavity created under the important strength of buoyancy, at $Ra_e = 10^5$, produces an increase in the mass flow rate through the cavity. Thus, the air temperature increases close to the top portion of the cold wall and decreases close to the bottom portion of the hot wall. Consequently, the convective contribution to the local Nusselt number is greater in the bottom region near the hot wall and in the top region near the cold wall, except in the case of the smaller opening size $H/4$, when the

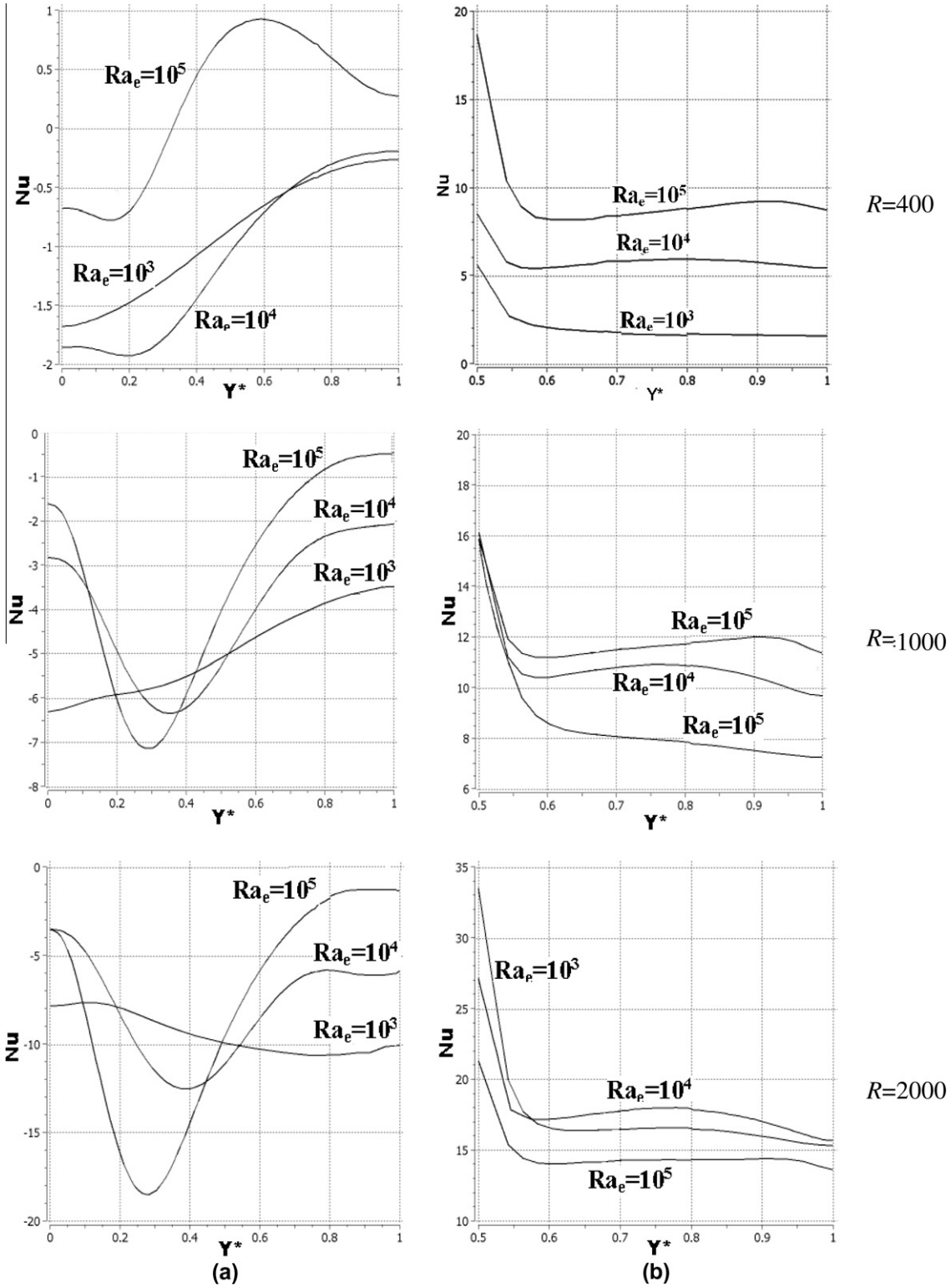

Fig. 11. Local Nusselt number along the (a) hot wall and (b) cold wall for an opening size of $H/2$.

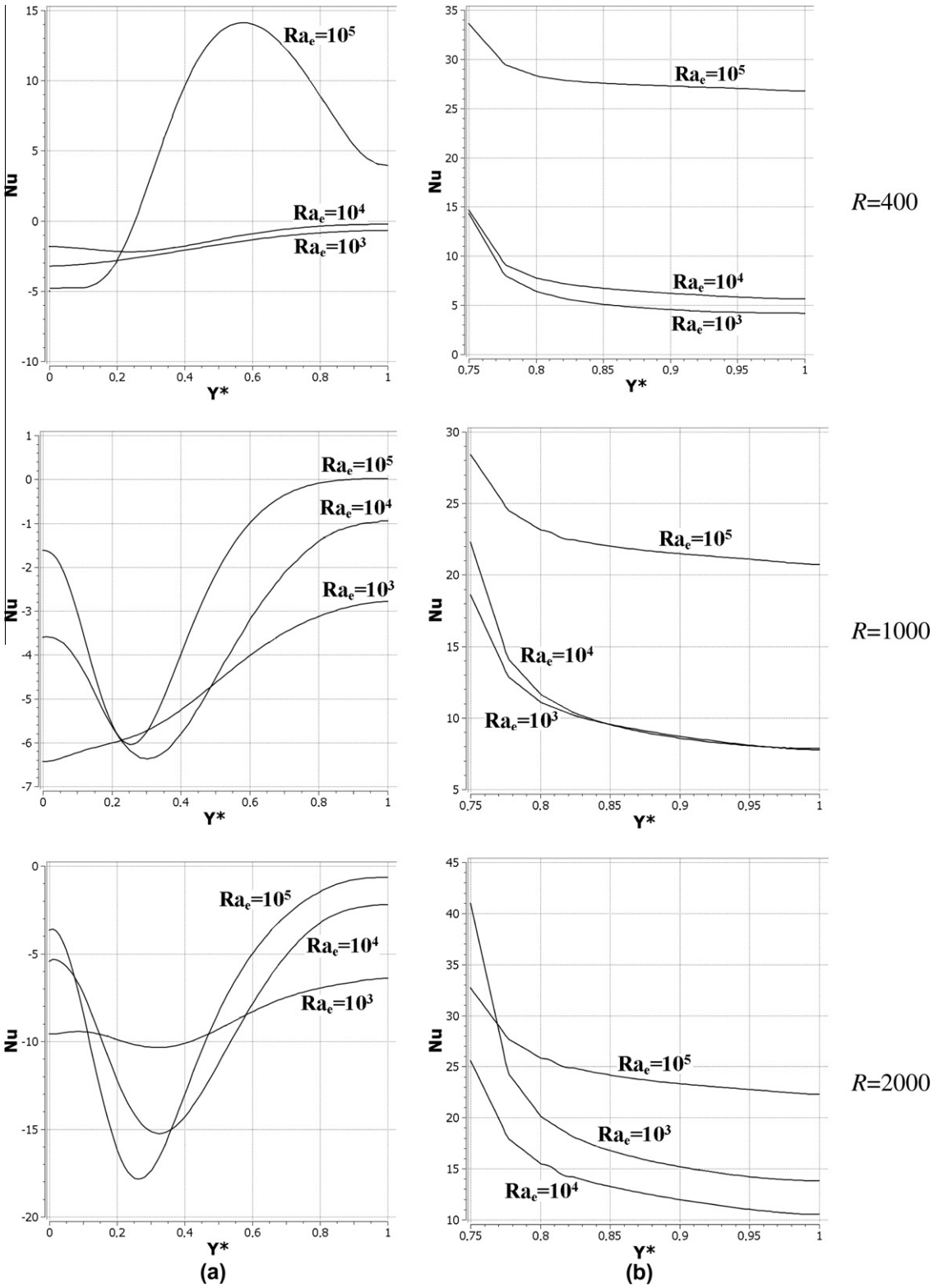

Fig. 12. Local Nusselt number along the (a) hot wall and (b) cold wall for an opening size of 3*H*/4.

air temperature increases in the upper region of the left cavity near the hot wall for larger Rayleigh numbers or *R* values. At the same time, the air temperature decreases in the lower region of the right cavity near the cold wall, thereby causing a decrease in the local Nusselt numbers in these regions only in the case of the smaller *R* values.

The effect of external Rayleigh numbers, Ra_e, and intensity of internal heat conduction source located in the center of the bottom wall on the heat transfer rate is shown in Fig. 10 for opening size *H*/4. The values for the local Nusselt number along the hot and cold walls are presented in Fig. 10 for opening size *H*/2 as a function of *R* and Ra_e. The local Nusselt number along the hot wall

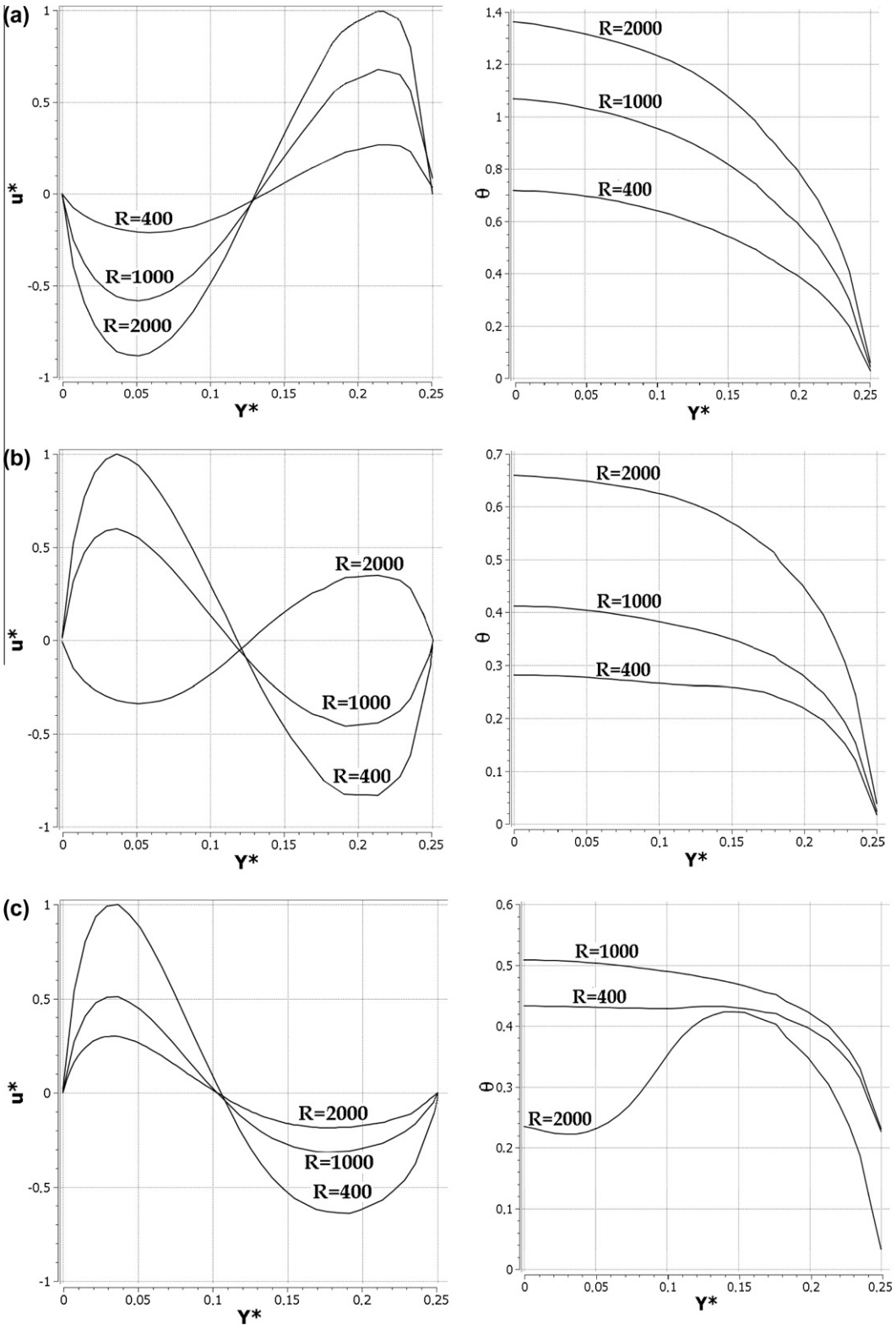

Fig. 13. Horizontal velocity (left) and temperature profiles (right) in the opening for (a) $Ra_e = 10^3$, (b) $Ra_e = 10^4$, and (c) $Ra_e = 10^5$ with an opening size of $H/4$.

(Fig. 10a) increases when $R = 400$ and this behavior changes when $R = 1000$ and 2000. Note that the local Nusselt curve along the hot wall in Fig. 10a, for opening size $H/4$, is very similar to the results for opening size $H/2$, as shown in Fig. 11a. The main difference between these figures can be noted for $R = 400$. However, in general, the phenomena governing the heat transfer along the hot wall are the same. Nevertheless, the values for local Nusselt number along the cold wall in Fig. 10b show appreciable difference in relation to those in Fig. 11b.

Fig. 10b shows the results for the local Nusselt number along the cold wall and for $R = 400$ and 1000 the behaviors are quite similar. However, when $Ra_e = 10^5$, the local Nusselt number is signifi-

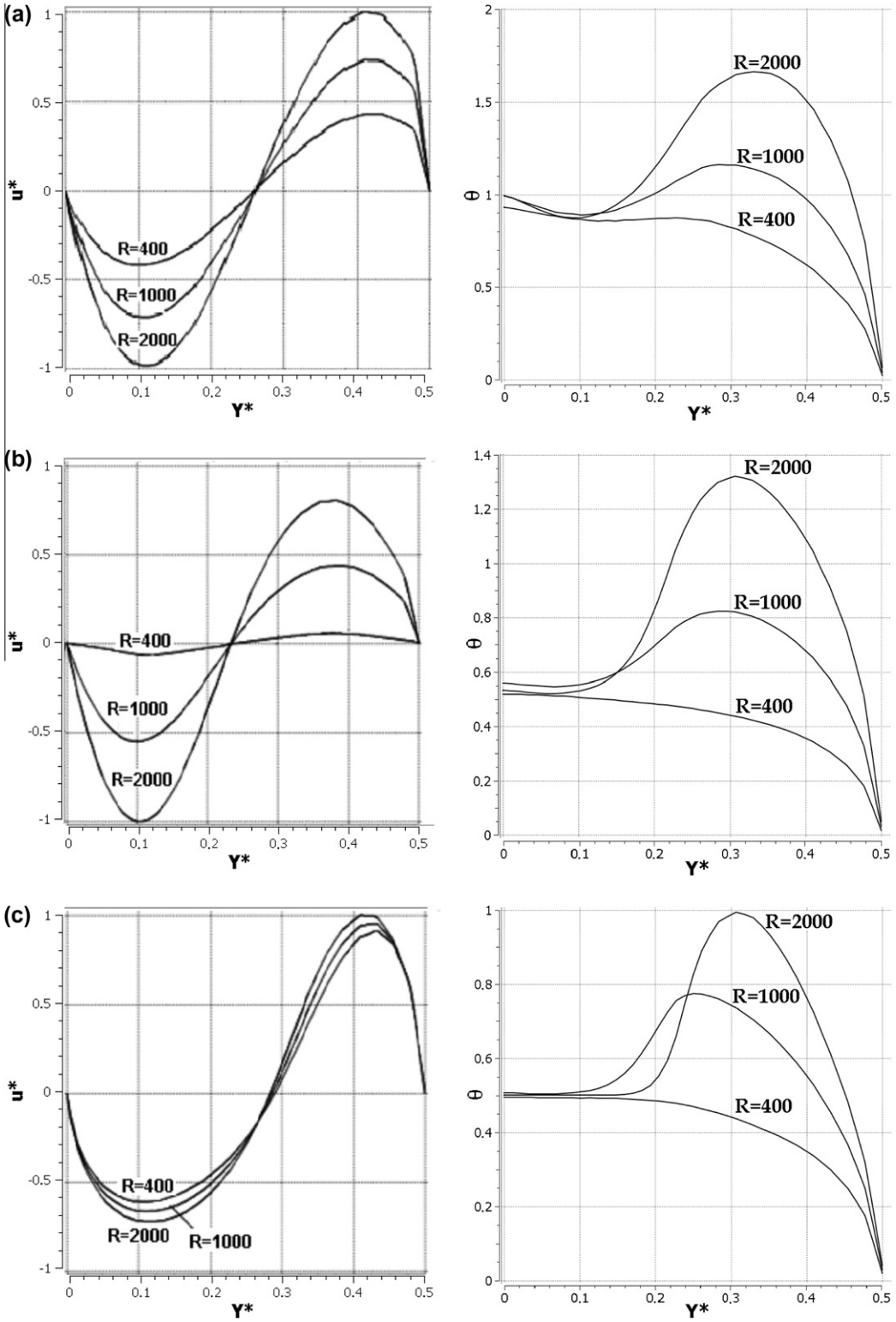

Fig. 14. Horizontal velocity (left) and temperature profiles (right), in the opening for (a) $Ra_e = 10^3$, (b) $Ra_e = 10^4$, and (c) $Ra_e = 10^5$ with an opening size of $H/2$.

cantly higher when compared to other values of Ra_e. Note that along the cold wall next to the opening ($Y^* = 0.2$) for $Ra_e = 10^3$ the local Nusselt number is higher than for $Ra_e = 10^4$. This occurs due to the heat source, its influence being more significant for an opening size of 25% because the beginning of the opening is next to the heat source.

In Fig. 10b, as expected, when $R = 400$ or 1000 it can be seen that Nu increases as a function of Ra_e, indicating that the intensity of heat transfer at the cold wall is a function of the temperature difference between the walls. In fact, analyzing the isotherms and flow lines, one can see that in these cases, the region close to the cold wall is little influenced by the heat source. When $R = 2000$ note that $Ra_e = 10^5$ gives the lowest values of Nusselt, while the maximum occurs when $Ra_e = 10^3$. In this case, the influence of the heat source becomes more evident, especially for small values of Ra_e, when the recirculation intensity is lower, and thus

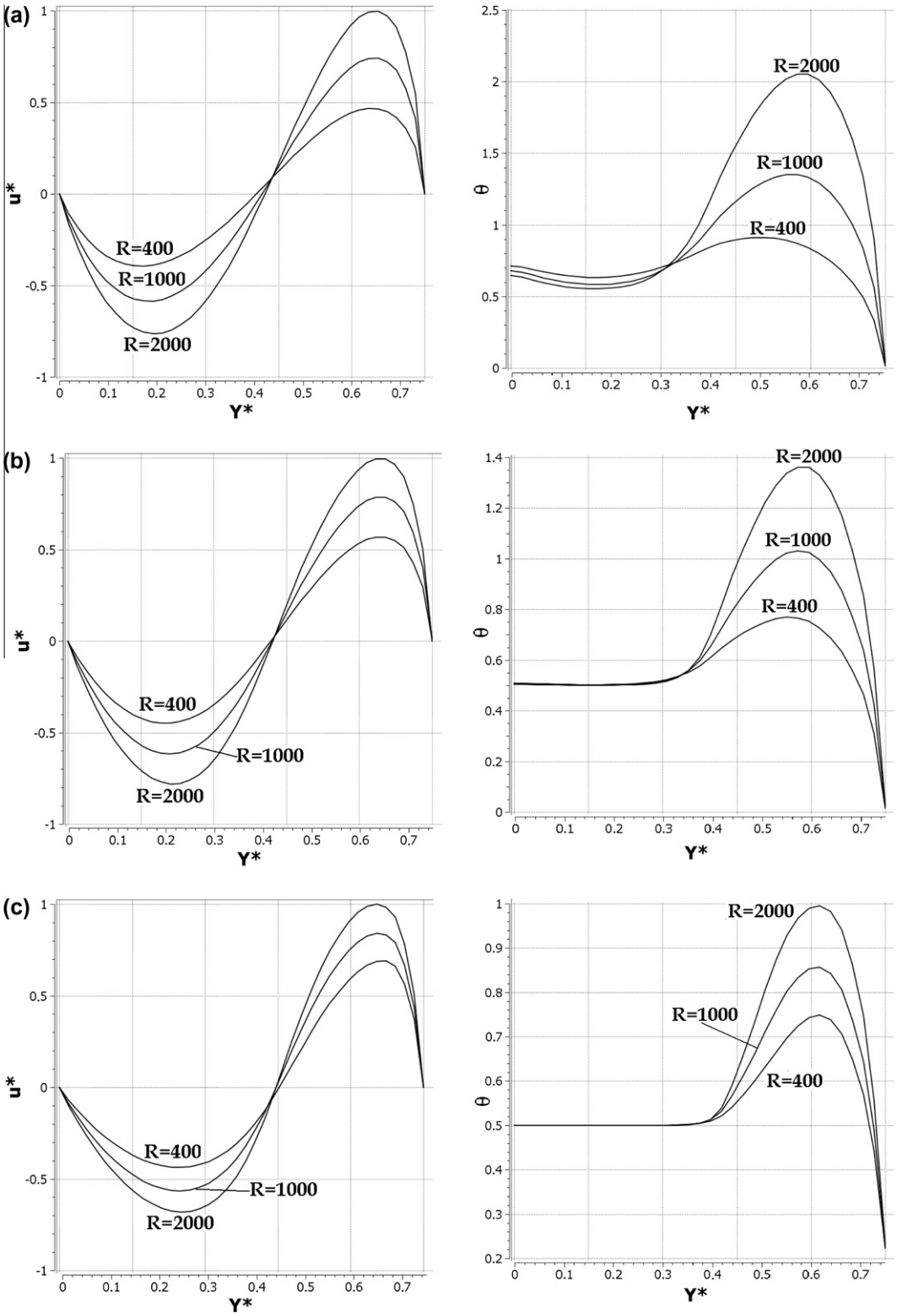

Fig. 15. Horizontal velocity (left) and temperature profiles (right) in the opening for (a) $Ra_e = 10^3$, (b) $Ra_e = 10^4$, and (c) $Ra_e = 10^5$ with an opening size of $3H/4$.

the dissipation of heat generated by the source does not greatly influence the air fluid dynamics. Therefore, the region at the bottom near the opening is heated more intensely, thus increasing the temperature gradient in relation to the cold wall.

The local Nusselt numbers along the hot and cold walls are shown in Fig. 11a and b, respectively, for opening size $H/2$ as a function of R and Ra_e. As shown in Fig. 11a the local Nusselt number increases with the distance Y^* along the hot wall for all Rayleigh numbers when $R = 400$, and decreases until approximately $Y^* = 0.4$, then increasing up to the top of the cavity when $R = 1000$ and 2000 for the larger Rayleigh numbers. This behavior of the variation of local Nusselt number can be attributed to the formation of secondary eddies and their increasing size with an increase in R and Ra_e. In Fig. 11b the local Nusselt number along the

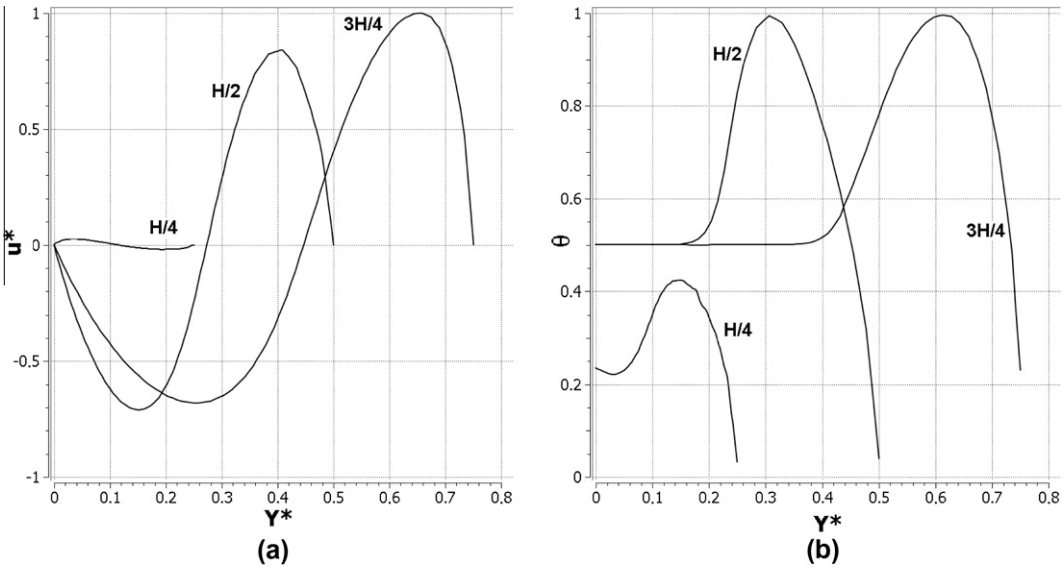

Fig. 16. (a) Horizontal velocity and (b) temperature profiles in the opening for various opening sizes, $Ra_e = 10^5$ and $R = 2000$.

cold wall is at a maximum near the opening wall and then decreases up to the top of the wall. For the cold wall, *Nu* decreases monotonically, since $Y^* = 0.5$, and even at approximately $Y^* = 0.6$, for all Rayleigh numbers. Thus, the main difference between Figs. 10 and 11 is the value of *Nu* along the cold wall.

The values for *Nu* in the cavity with an opening size of $3H/4$ can be seen in Fig. 12. For the hot wall (Fig. 12a) the values for $R = 400$ are significantly different from those for the other opening sizes, as in the previous case. This result shows that the opening size influences the heat transfer, along the hot wall, in the cases where the heat source is less relevant. On analyzing the local Nusselt number along the cold wall (Fig. 12b) the difference in comparison with the other opening sizes becomes more significant. For example, for $R = 400$, the behavior is quite similar to that observed for an opening of 25%, but for $R = 1000$, differences between the *Nu* values along the cold wall for $Ra_e = 10^3$ and 10^4 are very expressive in the region of the wall next to the opening, which is not observed for other opening sizes. Using $R = 2000$, a maximum *Nu* value at $Y^* = 0$ can be observed when $Ra_e = 10^3$, indicating the influence of the heat source.

Fig. 13 illustrates the profiles of the dimensionless horizontal velocity and temperature in the opening for various *R* and Ra_e values at an opening size of $H/4$. At a fixed lower Ra_e, when *R* increases, the portion of the opening occupied by the inflow becomes slightly smaller, the maximum dimensionless velocity and temperature become higher, and the position of the maximum outflow velocity and temperature move slightly towards the bottom of the wall. Note that when Ra_e increases this behavior is modified. At a fixed *R*, the change in the characteristics of the opening with Ra_e is more complex.

Fig. 14 plots the dimensionless horizontal velocity and temperature in the opening for various *R* and Ra_e values at an opening size of $H/2$. At a fixed Ra_e, when *R* increases, the portion of the opening occupied by the inflow becomes slightly smaller, the maximum dimensionless velocity and temperature become higher, and the position of the maximum outflow velocity moves slightly towards the bottom of the wall, while the position of the maximum temperature moves slightly towards the top of the wall. The inflow mass rate increases and the flow in the partially-open cavity becomes stronger at larger *R* or Ra_e values. A similar behavior is noted in Fig. 15 for dimensionless horizontal velocity and temperature with an opening size of $3H/4$. However, in this figure the temperature becomes constant for approximately half of the opening and the position of the maximum temperature moves towards the top of the wall.

In Fig. 16 the horizontal velocity and temperature profiles in the opening, for different opening sizes, are shown for $Ra_e = 10^5$ and $R = 2000$. Note that when the opening size is small, the part of the opening occupied by the inflows is smaller than that occupied by the outflow. With an increase in the opening size the former becomes larger, and for the largest opening size the former is larger than the latter. The maximum dimensionless velocity and the inflow mass rate increase with opening size, but the maximum dimensionless temperature undergoes a complex change with opening size, particularly in the case of the smallest opening.

5. Conclusions

This study investigated the variations in the streamlines and isotherms of a square cavity as a function of different values of internal and external Rayleigh numbers. The cavity has an opening on the right wall and a small heat source located on the bottom wall, occupying the central position. The phenomenon of natural convection was evaluated for values of Ra_e between 10^3 and 10^5, values of *R* between 400 and 2000, and three configurations of the opening in the right vertical wall of the cavity, $H/4$, $H/2$ and $3H/4$.

The results show that the thermal and fluid dynamics of the fluid are highly influenced by the presence of the heat source, by the opening size and by the temperature difference between the vertical walls. When the flow is controlled mainly by the heat source (high values of *R* and low values of Ra_e) there are large secondary circulations inside the cavity and the isotherms exhibit parabolic behavior, causing an increase (in modulus) in the values of local Nusselt number. When the natural convection is controlled by the temperature difference between the walls (low values of *R* and high values of Ra_e), the size of the secondary circulation is negligible in comparison to the main recirculation and the isotherms are more horizontal. The convective contribution to the local Nusselt-number is augmented in the bottom region near the hot wall and in the top region near the cold wall, except for the smaller size opening $H/4$ when the air temperature increases in the higher region of the cavity near the hot wall for larger Rayleigh numbers and larger *R* values. At the same time, the air temperature decreases in the lower region to the right of the cavity near the cold

wall, thereby causing a decrease of the local Nusselt numbers in these regions only in the case of lower R values.

Acknowledgment

The last author would like to thanks CNPq (Conselho Nacional de Desenvolvimento Científico e Tecnológico – Brazil) (processes: 568221/2008-7, 474408/2008-6, PQ/302786/2008-2, 475689/2010-0) for its financial support of this work.

References

[1] I. Sezai, A.A. Mohamad, Suppressing free convection from a flat plate with poor conductor ribs, Int. J. Heat Mass Transfer 42 (1998) 2041–2051.
[2] T. Pesso, S. Piva, Laminar natural convection in a square cavity: low Prandtl numbers and large density differences, Int. J. Heat Mass Transfer 52 (2009) 1036–1043.
[3] T. Zitzmann, M.P. Cook, P. Pfrommer, S. Rees, L. Marjanovic, Simulation of steady state natural convection using CFD, in: Proceeding of Building Simulation, Montreal, Canada, 2005, pp. 1–8.
[4] V.A.F. Costa, Thermodynamic of natural convection in enclosures with viscous dissipation, Int. J. Heat Mass Transfer 48 (2005) 2333–2341.
[5] G.V. Davis, Natural convection of air in a square cavity: a bench mark numerical xolution, Int. J. Numer. Methods Fluids 3 (2005) 249–264.
[6] B. Abourida, M. Hasnaoui, S. Douamma, Natural convection in a square cavity with vertical boundaries submitted to periodic temperatures, Rev. Gen. Therm. 37 (1998) 788–800.
[7] B.S. Yilbas, S.Z. Shuja, S.A. Gradebo, H.I. Al-Hamayel, K. Boran, Natural convection and entropy generation in a square cavity, Int. J. Energy Res. 22 (1998) 1275–1290.
[8] G. Barakos, E. Mitsoulis, D. Assimacopoulos, Natural convection flow in a square cavity revisited: laminar and turbulent models with walls functions, Int. J. Numer. Methods Fluids 18 (2005) 695–719.
[9] B.A.V. Bennett, J. Hsueh, Natural convection in a cubic cavity: implicit numerical solution of two benchmark problems, Numer. Heat Transfer A Appl. 50 (2006) 99–123.
[10] R.S. Kaluri, T. Basak, S. Roy, Bejan's heatlines and numerical visualization of heat flow and thermal mixing in various differentially heated porous square cavities, Numer. Heat Transfer A Appl. 55 (2009) 487–516.
[11] Q.H. Deng, J.J. Chang, Natural convection in a rectangular enclosure with sinusoidal temperature distributions on both side walls, Numer. Heat Transfer A Appl. 54 (2008) 507–524.
[12] T. Michalek, High Rayleigh number natural convection in a cubic enclosure, in: Proceeding of Eurotherm Seminar of Numerical Heat Transfer, Gliwice-Cracow, Poland, 2005, pp. 1–11.
[13] E. Bilgen, H. Oztop, Natural convection heat transfer in partially open inclined square cavities, Int. J. Heat Mass Transfer 48 (2005) 1470–1479.
[14] F. Kuznik, J. Vareilles, G. Rusaouen, G. Krauss, A double-population lattice Boltzmann method with non-uniform mesh for the simulation of natural convection in a square cavity, Int. J. Heat Fluid Flow 28 (2007) 862–870.
[15] A. Mezrhab, M. Jami, C. Abid, M. Bouzidi, P. Lallemand, Lattice–Boltzmann modelling of natural convection in an inclined square enclosure with partitions attached to its cold wall, Int. J. Heat Fluid Flow 27 (2006) 456–465.
[16] A. Bahlaoui, A. Raji, R. El Ayachi, M. Hasnaoui, M. Lamsaadi, M. Naïmi, Coupled natural convection and radiation in a horizontal rectangular enclosure discretely heated from below, Numer. Heat Transfer A Appl. 52 (2007) 1027–1042.
[17] R. El Ayachi, A. Raji, M. Hasnaoui, A. Bahlaoui, Combined effect of radiation and natural convection in a square cavity differentially heated with a periodic temperature, Numer. Heat Transfer A Appl. 53 (2008) 1339–1356.
[18] J.F. Hinojosa, C.A. Estrada, R.E. Cabanillas, G. Alvarez, Numerical study of transient and steady-state natural convection and surface thermal radiation in a horizontal square open cavity, Numer. Heat Transfer A Appl. 48 (2005) 179–196.
[19] G.V. Kuznetsov, M.A. Sheremet, Conjugate heat transfer in an enclosure under the condition of internal mass transfer and in the presence of the local heat source, Int. J. Heat Mass Transfer 52 (2009) 1–8.
[20] A.B. Nakhi, A.J. Chamkha, Conjugate natural convection around a finned pipe in a square enclosure with internal heat generation, Int. J. Heat Mass Transfer 50 (2007) 2260–2271.
[21] H. Oztop, E. Bilgen, Natural convection in differentially heated and partially divided square cavities with internal heat generation, Int. J. Heat Fluid Flow 27 (2006) 466–475.
[22] H.F. Oztop, E. Abu-Nada, Numerical study of natural convection in partially heated rectangular enclosures filled with nanofluids, Int. J. Heat Fluid Flow 29 (2008) 1326–1336.
[23] A. Bazylak, N. Djilali, D. Sinton, Natural convection in an enclosure with distributed heat sources, Numer. Heat Transfer A Appl. 49 (2006) 655–667.
[24] É. Fontana, A. Silva, V.C. Mariani, F. Marcondes, The influence of baffles on the natural convection in trapezoidal cavities, Numer. Heat Transfer A Appl. 58 (2010) 125–145.
[25] S. Sivasankaran, C.J. Ho, Buoyancy- and thermocapillary-induced convection of cold water in an open enclosure with variable fluid properties, Numer. Heat Transfer A Appl. 58 (2010) 457–474.
[26] T.H. Hsu, K.Y. Hong, Natural convection of micropolar fluids in an open cavity, Numer. Heat Transfer A Appl. 50 (2006) 281–300.
[27] A. Andreozzi, O. Manca, Numerical investigation on the steady state natural convection in a horizontal open-ended cavity with a heated upper wall, Numer. Heat Transfer A Appl. 57 (2010) 453–472.
[28] V.C. Mariani, A. Silva, Natural convection: analysis of partially open enclosures with an internal heated source, Numer. Heat Transfer A Appl. 52 (2007) 595–619.
[29] V.C. Mariani, L.S. Coelho, Partially open enclosures containing an internal local heat source, Braz. J. Chem. Eng. 24 (2007) 375–388.
[30] P. Kandaswamy, J. Lee, A. Hakeem, Natural convection in a square cavity in the presence of heated plate, Nonlinear Anal. Model. Control 12 (2007) 203–212.
[31] M. Hortmann, M. Peric, G. Scheuerer, Finite volume multigrid prediction of laminar natural convection: benchmark solutions, Int. J. Numer. Methods Fluids 11 (1990) 189–207.
[32] J.L. Xia, Z.W. Zhou, Natural convection in an externally heated partially open cavity with a heated protrusion, FED-vol. 143/HTD, Measurement and Modeling of Environmental Flows – ASME, vol. 232, 1992, pp. 201–208.